JOURNAL OF GEOPHYSICAL RESEARCH, VOL. 114, F03017, doi:10.1029/2008JF001142, 2009

Influence of steady base-level rise on channel mobility, shoreline migration, and scaling properties of a cohesive experimental delta

John Martin,[1,2] Ben Sheets,[2,3] Chris Paola,[1] and David Hoyal[2]

Received 26 September 2008; revised 31 March 2009; accepted 6 May 2009; published 29 August 2009.

[1] Here we describe results from an alluvial delta physical experiment with and without steady base-level rise. Using a unique cohesive sediment mixture that promotes the development of persistent channels and a rugose shoreline, we quantitatively characterize channel network properties as a function of base-level rise in a distributary system that reproduces many aspects of the geometry of natural deltas. Analysis of the experimental data shows clear dynamical differences between the predominantly progadational and aggradational phases of the experiment. The experiment was conducted in two phases: a first in which the delta prograded into standing water of constant depth in the absence of base-level rise and a second during which steady base-level rise was imposed on the system, forcing a twofold increase in topset aggradation due to greater sediment retention in the fluvial reach. The shift in sediment mass balance to enhanced fluvial deposition in the second phase caused channel network mobility to increase, reducing the autogenic channel time scale from 23.5 to 12.5 h and supporting a positive correlation between deposition and channel avulsion frequency. An independent shoreline time scale that characterizes the dominant time over which shoreline regression is persistent closely correlates with measurements of the channel network (28.3 h during fan progradation and 9.5 h during fan aggradation). These metrics suggest a strong coupling between channel network and shoreline kinematics and a more active fluvial surface during fan aggradation by a factor of 2 to 3, similar to the increase in aggradation rate. Spatial scaling of shoreline roughness reveals that maximum shoreline variability is set by the scale of distributary lobes. Strong coupling exists between delta growth and shoreline geometry during progradation. During aggradation, however, shoreline variability is not solely due to distributary lobe growth but is also set by shoreline transgression over inactive portions of the delta, illustrating a decoupling between fan kinematics and fan geometry. This decoupling, together with the matched increase in channel network mobility and fluvial aggradation, suggest the stratigraphic architecture may not be a strong geometric signal of different fluvial surface conditions either.

Citation: Martin, J., B. Sheets, C. Paola, and D. Hoyal (2009), Influence of steady base-level rise on channel mobility, shoreline migration, and scaling properties of a cohesive experimental delta, *J. Geophys. Res.*, *114*, F03017, doi:10.1029/2008JF001142.

1. Introduction

[2] Physical stratigraphy reflects the interplay of the (static) geometric properties of depositional surfaces; the kinematics of these surfaces; and net deposition or erosion driven by external processes like subsidence and sea level change. Study of modern depositional environments provides abundant information about static spatial geometry and how this is linked to other key properties like grain size. If they are sufficiently active, they can also provide some information about kinematics. In rare cases, we can even obtain information on long-term rates of deposition and erosion. But in general, to observe the full range of interactions among surface geometry, surface kinematics, and net deposition that create physical stratigraphy, we must use laboratory experiments and/or numerical models, two ways of, in effect, "speeding up time."

[3] A key issue in this context is how surface geometry and kinematics are coupled to net deposition. For example, *Leeder* [1978] obtained his well known inverse relation between cross-sectional stacking density and rate of deposition by assuming that the avulsion frequency (the kinematic parameter) is independent of subsidence rate. This was later shown to be incorrect by *Bryant et al.* [1995], who pointed out that qualitatively the relation between sedimentation rate and stacking density depends on the strength of the coupling between avulsion frequency and rate of deposition.

[1] St. Anthony Falls Laboratory and Department of Geology and Geophysics, University of Minnesota, Minneapolis, Minnesota, USA.
[2] ExxonMobil Upstream Research Company, Houston, Texas, USA.
[3] School of Oceanography, University of Washington, Seattle, Washington, USA.

0148-0227/09/2008JF001142$09.00

[4] Most natural transport systems display at least some degree of stochastic behavior that unfolds over multiple scales of space and time [*Gomez et al.*, 1989; *Ashmore*, 1991; *Paola and Foufoula-Georgiou*, 2001; *Jerolmack and Paola*, 2007]. In these cases, a single kinematic parameter (e.g., an avulsion frequency) will generally not be sufficient to incorporate the full suite of kinematics that control stratal patterns. In this paper, we use a physical experiment involving a novel, weakly cohesive sediment mix to (1) develop an initial set of quantitative descriptors to capture the spatial pattern and kinematics of stochastic deltaic distributary networks and (2) investigate how these parameters are influenced by rate of deposition controlled by base-level rise.

[5] The key to understanding boundary effects on shoreline geometry and distributary channel dynamics is through detailed quantification of time and length scales, which measure relative mobility of characteristic phenomena such as channels, sediment distribution, and the shoreline itself, all of which are reflected in both the channel network topology [e.g., *Morisawa*, 1985; *Edmonds and Slingerland*, 2007] and coastline morphology [e.g., *Hoyal and Sheets*, 2009]. Previous studies of deltaic dynamics, however, have generally focused on the interaction between standing water and distributary channels very near the coastline. For example, *Wright* [1977], following on the seminal work of *Bates* [1953], considered the range of fluid dynamic forces acting on river mouth effluent, including buoyancy, friction, and inertia. Their work, however, did not generally consider the evolving interaction between incipient topography and effluent, much less interaction with the channel network. *Wright and Coleman* [1973] considered the morphological influence of a wider range of coastal zone transport processes, work culminating in the classic wave-tide-river ternary diagram of deltaic morphology, but generally considered the influence of these processes on only the coastline morphology. Since the publication of these studies, the influence of coastal processes on the channel system has been recognized, but generally treated in a necessarily simplified manner [e.g., *Swenson*, 2005]. Recent experimental studies have documented a strong interaction between coastal processes and channel network morphology [*Kim et al.*, 2006; *Hoyal and Sheets*, 2009].

[6] Distributary channel dynamics are perhaps best understood for cases in which downstream controls are negligible or absent. For example, there is a large body of research focused on alluvial avulsion dynamics, which are intimately related to the time and length scales of interest here. Such studies have led to emerging semiquantitative theories regarding channel relocation [e.g., *Bryant et al.*, 1995; *Heller and Paola*, 1996; *Slingerland and Smith*, 1998, 2004; *Mohrig et al.*, 2000; *Tornqvist and Bridge*, 2002; *Jerolmack and Mohrig*, 2007]. Further, these alluvial situations provide a base case for investigating the influence of allogenic forcing on autogenic behavior. For example, the effect of variable subsidence pattern and rate on autogenic dynamics has been addressed in a number of experimental [e.g., *Cazanacli et al.*, 2002; *Hickson et al.*, 2005; *Kim and Paola*, 2007], numerical [e.g., *Sun et al.*, 2002] and field studies [e.g., *Alexander and Leeder*, 1987; *Leeder et al.*, 1996; *Peakall et al.*, 2000].

[7] Here our motivation is to begin quantifying the kinematic and geometric linkages between coastline and distributary channel network phenomena that evolve in a distributive system with geometric properties similar to natural deltas. First, we explore characteristic (i.e., averaged) time scales related to channelized delta processes under distinct basinal sediment mass balance regimes forced by base-level rise. Second, we compare this to independent measures of shoreline migration in order to evaluate channel network and shoreline coupling in the absence of strong offshore reworking. Third, we use channel and shoreline time scale information to explore the imprint of delta kinematics on shoreline geometry, the primary metric of external form in deltaic distributive systems.

2. Experimental Methods

[8] The experimental delta, hereafter referred to as DB07, was run at St. Anthony Falls Laboratory, University of Minnesota, in the Delta Basin experimental facility. The basin is $5 \times 5 \times 0.62$ m in size and is designed for constructing alluvial fan deltas where uniform subsidence is an adequate boundary condition (Figure 1a). Base level is modulated by a computer-controlled weir and attached siphon at the opposite side of the basin, and water and sediment supply are independently controlled through a computer-operated centrifugal pump and sediment feeder, respectively.

[9] DB07 was designed to explore autogenic processes within a well channelized distributary system as a function of steady base-level rise. During the 200-h experiment, a constant supply of water ($Q_{w0} = 0.167$ l s^{-1}) and sediment ($Q_{s0} = 1.7 \times 10^{-4}$ l s^{-1}) were mixed and delivered to the basin as a slurry through a narrow inlet channel. The experiment was run in two equal length stages of 100 h. In stage one the delta prograded into a standing body of water constant depth ($H_w = 30$ mm) and no base level rise or subsidence. In stage two we induced constant, uniform base level rise ω equal to 0.28 mm h^{-1}, which was matched to the sediment supply so as to maintain the averaged fan radius of approximately 1100 mm established at the end of stage one (Figure 1c). The streamwise alluvial slope S_A is a self-formed property of the experimental delta [e.g., *Paola et al.*, 1999] and has a characteristic value of about 0.03. To allow measurement of wetted area and distinguish channel, floodplain flow geometry from surface images, the flow was dyed blue and made opaque by adding a small amount of fine-grained titanium dioxide.

[10] The sediment used in DB07 is a mixture that ranges uniformly from bentonite clay to coarse sand. Added to this is a small amount of a commercially available polymer that increases the mixture cohesiveness, which in turn promotes the development and maintenance of stable channels (a thorough description of the sediment mix is outlined by *Hoyal and Sheets* [2009]). This sediment mixture, developed at ExxonMobil Upstream Research, is an important breakthrough in experimentation since it extends our ability to document fan delta morphodynamics to include relatively stable, distributary channel networks, in contrast to the braided networks typical of noncohesive experimental deltas [e.g., *Cazanacli et al.*, 2002].

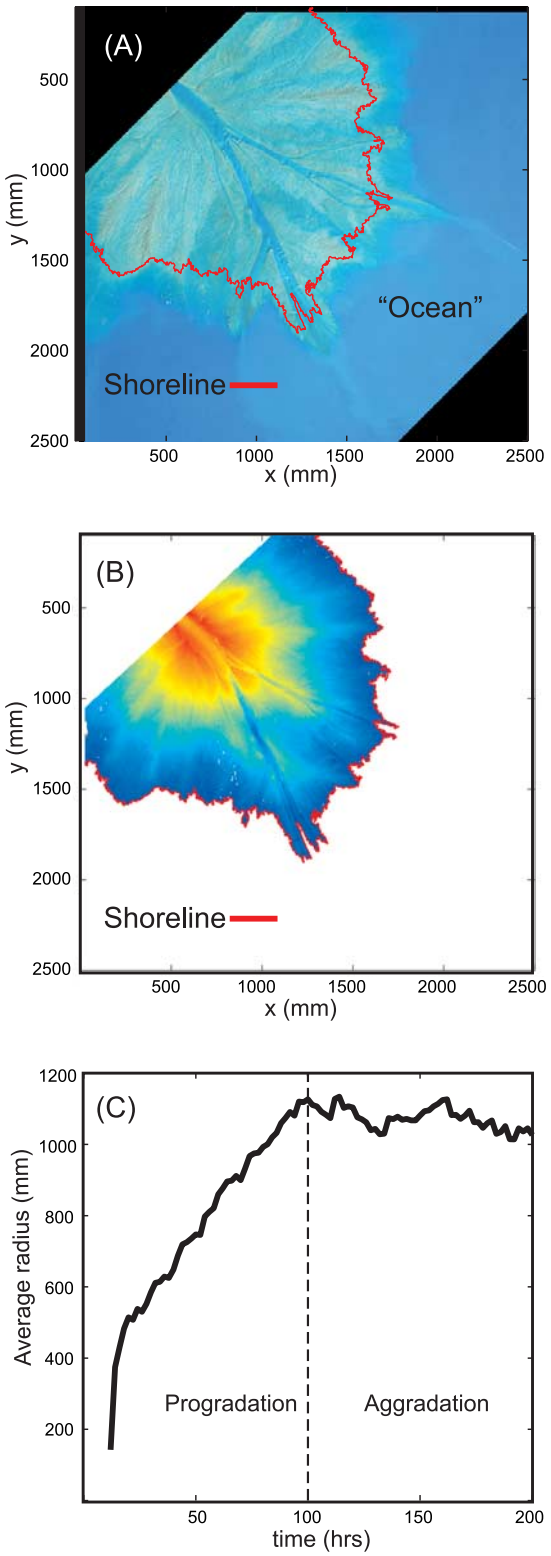

Figure 1. (a) Overhead image of DB07. Water and sediment supply source is at upper left. Image is geometrically rectified and is in the same coordinate space as topography scans, as demonstrated by the topographic shoreline contour drape in red. (b) Corresponding topographic scan of image in Figure 1a (note similarity in flow pattern). (c) Average fan radius over the course of the experiment.

[11] Overhead photos of the experimental surface were taken every 30 s. Additionally, highly resolved (5 × 5 × 0.1 mm) laser topography scans were collected over the alluvial surface every 2 h (Figure 1b). At the end of the experiment, the deposit was serially sectioned every 100 mm and cored at five equally spaced, collinear locations midway between each exposed face.

3. Surface Observations of a Cohesive Experimental Delta

[12] Before moving on to the details of the analysis, it is worth underscoring the surface effects from a weakly cohesive sediment mixture. The primary morphodynamic outcome of cohesion is to restrict channel sidewall erosion and channel widening, which suppresses the braided channel instability in favor of single thread channels. This results in several important kinematic and network differences between channelized cohesive and noncohesive experimental deltas (Figure 2). First and perhaps most obvious, cohesion leads to relatively low aspect ratio channels that are more persistent geomorphic features. Greater flow depths relative to channel width and the presence of fine-grained sediment result in suspended load sediment transport, overbank sedimentation, and levee formation. This creates a surface motif of clearly differentiated flow between channels and overbank (Figures 2a–2d).

[13] Second, restricted flow mobility limits flow expansions as unconfined sheet flow, which is a common depositional flow configuration in braided environments [*Sheets et al.*, 2002]. Flow expansion in cohesive experiments is more generally through branching distributary channels, which gives rise to a channelized structure much more akin to natural deltas (Figures 2e and 2f). This difference is significant since sheet flow often converges in flow confluences, another common channel-braiding dynamic [*Paola*, 2001]. Consequently, unlike noncohesive distributary systems, where the frequency of bifurcations and confluences is similar, in cohesive environments the frequency of flow bifurcations is much greater than confluences (Figures 2g and 2h). We quantify this point by deriving the cumulative probability function of the number active channel confluences N_C and bifurcations N_B, $F(N_C)$ and $F(N_B)$, between this and a representative noncohesive delta (described in detail by *Kim et al.* [2006]), where in each delta these flow configurations were manually picked. In order to represent the two experiments equally, we measure these events over an equilibrium basin time scale defined by $T_E = L_f^2/\upsilon$, where L_f is the delta length and υ is a physically based diffusion coefficient [*Paola et al.*, 1992, 1999]. Here υ is defined as $\upsilon = q_{s0}/S_A$, where q_{s0} is the mean sediment supply to the system along an arbitrary streamwise transect and is approximated by $q_{s0} = Q_{s0}/\overline{B}_{\sum ch}$, where $\overline{B}_{\sum ch}$ is the mean summed channel width. Distribution results are shown in Figure 2g, where we find that the median M number of active flow confluences and bifurcations are close in the noncohesive delta ($MN_{C,nc} = 2.0$; $MN_{B,nc} = 2.7$) and demonstrably divergent in the cohesive delta ($MN_{C,c} = 0.5$; $MN_{B,c} = 7.4$).

[14] Third, the more persistent and hierarchical channel network in the cohesive delta promotes a shoreline contour that exhibits much greater roughness (i.e., variability) than

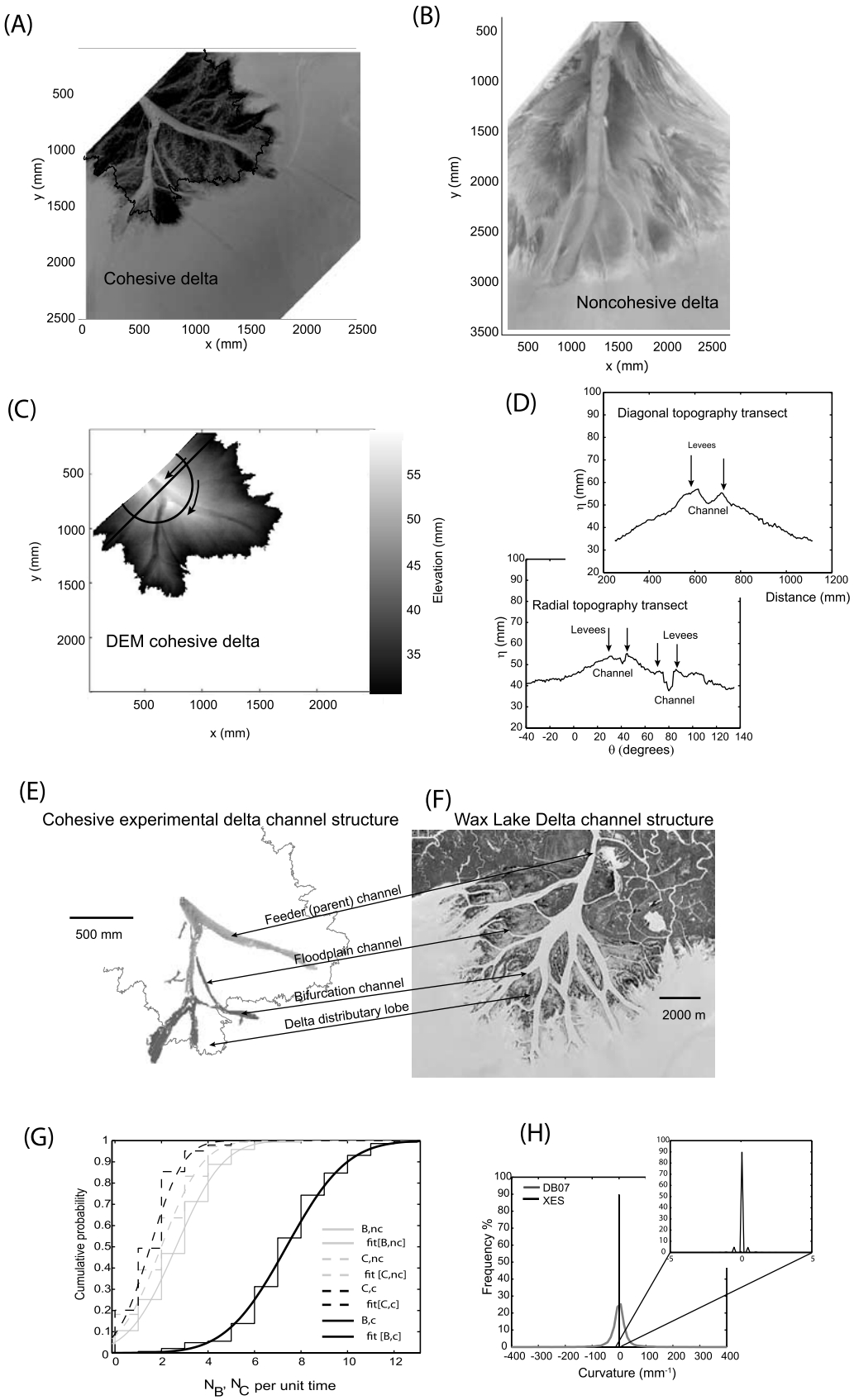
(A)
Cohesive delta
y (mm)
x (mm)
(B)
Noncohesive delta
y (mm)
x (mm)
(C)
DEM cohesive delta
Elevation (mm)
y (mm)
x (mm)
(D)
Diagonal topography transect
Levees
Channel
η (mm)
Distance (mm)
Radial topography transect
Levees
Levees
Channel
Channel
η (mm)
θ (degrees)
(E)
Cohesive experimental delta channel structure
500 mm
Feeder (parent) channel
Floodplain channel
Bifurcation channel
Delta distributary lobe
(F)
Wax Lake Delta channel structure
2000 m
(G)
Cumulative probability
B,nc
fit[B,nc]
C,nc
fit [C,nc]
C,c
fit[C,c]
B,c
fit [B,c]
N_B, N_C per unit time
(H)
DB07
XES
Frequency %
Curvature (mm⁻¹)

Figure 2

the braided example. This effect is obvious in Figures 2a and 2b and easily quantified by calculating the distribution of shoreline curvature (Figures 2g and 2h). The much larger distribution of shoreline curvature in the cohesive experiment indicates that, insofar as variability in the shoreline reflects the degree of channelization (in the absence of offshore processes), the shoreline structure is a sensitive mirror of gross properties of the fluvial system.

4. Equilibrium Base-Level Rise, Sedimentation, and Avulsion Frequency

[15] Our goal in the paper is to explore how shifts in deltaic sediment mass balance, driven by base-level rise, affect channel and shoreline migration kinematics. Previous work has focused on the correlation between sediment supply (and not specifically on the distribution of sediment) and channel avulsion for experimental alluvial fan deltas [*Bryant et al.*, 1995] and braided rivers [*Ashworth et al.*, 2004]. For example, *Bryant et al.* [1995] reasoned that superelevation of a channel above its floodplain is a common condition leading to avulsion due to higher sedimentation rates near the channel than farther out on the floodplain. In principle, however, the presence of aggradation forced by either subsidence or base-level rise should result in a similar effect by inducing greater topset deposition. This has been shown for the Holocene Rhine-Meuse Delta by *Tornqvist* [1994], who measured greater avulsion frequency during an episode of faster sea level rise and delta aggradation.

[16] A simple base-level rise case that can serve as a reference for comparison is one where the base-level rise rate (ω) balances the total sediment supply Q_{s0} and fan area A_f, such that $\omega = Q_{s0}/C_0A_f$ where C_0 is the volumetric sediment concentration in the deposit. We term this condition equilibrium base-level rise since on average this results in a purely aggradational fan delta. The effect of equilibrium base-level rise on sediment mass balance, which is expressed in the alluvial aggradation rate, is significant as shown by the following geometric considerations. In the experimental delta, under conditions of pure progradation the alluvial aggradation rate is formulated as

$$\dot{\eta}_{\text{prog}} = \left\{ q_{s0} \Big/ \left[\underbrace{L_f}_{\text{fluvial}} + \left(\underbrace{H_w/S_s}_{\text{marine}} \right) \right] \right\}, \tag{1}$$

where $\dot{\eta}$ is the time rate of change of the alluvial surface elevation, S_s is slope of the submarine delta foreset (approximately angle of repose), L_f is again the fan length, and H_w is the water depth. In (1), aggradation is limited by the fan length over which the given supply must deposit, as well as the amount of bypassed sediment that is stored in marine clinoforms. With equilibrium base-level rise, in an averaged sense most of what would be bypassed sediment is sequestered in the fluvial reach to maintain a constant shoreline position during relative base-level rise. In this case

$$\dot{\eta}_{agg} = \left[q_{s0} \Big/ \left(\underbrace{L_f}_{\text{fluvial}} + \underbrace{0}_{\text{marine}} \right) \right], \tag{2}$$

resulting in $\dot{\eta}_{agg} > \dot{\eta}_{prog}$. By using the experimental parameters in Table 1 we find that $\dot{\eta}_{agg}/\dot{\eta}_{prog} = 1.9$, an approximately twofold increase in the alluvial sedimentation rate. Direct measurement of delta aggradation rates yields a slightly smaller ratio ($\sim$1.7).

Table 1. Experimental Parameters From DB07

Q_w (l s^{-1})	Q_s (l s^{-1})	Q_w/Q_s	L_f (mm)	H_w (mm)	S_A	ω (mm h^{-1})
0.167	1.7×10^{-4}	$\sim$1000	1100	30	0.03	0.28

5. Channel Time Scale Analysis

[17] Gaining clear insight into the surface effects of variable sediment mass balance in DB07 requires us to measure key properties of a self-formed, evolving channel network. *Jerolmack and Mohrig* [2007] have shown that to first order the number of active channel branches (an important surface property) is actually scaled by process-based rates: the ratio of lateral migration to fluvial aggradation. Given their results, a measure of channel mobility is a valuable quantity to know. However, even in a small, well constrained setting, a freely evolving flow pattern presents a difficult quantity to assess. Despite well channelized and persistent flow paths, channel avulsion and lateral migration are end-member processes in a spectrum of flow dynamics. Hence, labeling an avulsion sensu stricto [e.g., *Slingerland and Smith*, 2004], for example, is not always possible. Here, we bypass this issue by deriving a channel time scale on the basis of quantifying the progressive loss of flow pattern similarity, a decorrelation, between an arbitrary reference image and successive images [*Wickert*, 2007].

5.1. Measuring Channel Mobility

[18] Decorrelation analysis is outlined in detail by *Wickert* [2007], so for our purposes here the details are kept to a minimum. Channel decorrelation is performed by extracting binary maps of the channel pattern (i.e., channel = 1, overbank = 0) over a constant fluvial domain from the overhead images using a constant threshold saturation of the dyed water to indicate a "channelized" pixel. A given reference binary map is then compared to a consecutive

Figure 2. Comparison of cohesive and noncohesive experimental deltas. Inverted gray scale images of (a) DB07 and (b) representative noncohesive experiment. (c) DB07 topographic scan corresponding to the image in Figure 2a and (d) two topographic transects across the fan illustrating channel and levee topography. Similar channel organization between (e) DB07 and (f) Wax Lake Delta. Image of Wax Lake Delta is from http://maps.google.com. (g) Quantitative evaluation between DB07 and noncohesive experiment concerning the average number of active channel bifurcations and confluences and (h) the frequency distribution of shoreline curvature. Subscripts *C* and *B* refer to "confluence" and "bifurcation," and *nc* and *c* refer to "noncohesive" and "cohesive," respectively.

series of maps through time, in this application $0 \leq \Delta t \leq 40$ h. The total number of changed pixels, when divided by total number of image domain pixels and subtracted from 1 is the total correlation ρ (where $0 \leq \rho \leq 1$) between the reference image ($\Delta t = 0$) and an arbitrarily chosen sample image in the time domain $0 < \Delta t \leq 40$ h. After including a normalization parameter [cf. *Wickert*, 2007], over time, as the flow pattern changes from its initial state at $t = 0$, ρ decays from its initial value of 1 to approximately 0. *Wickert* [2007] has shown that the decay in flow pattern for other experimental braided channel systems is approximately exponential.

[19] Given the need for both a significant fluvial area to perform this analysis and a 40-h time window for each reference image, we map decorrelation for the progradation phase between 50 and 60 h (the fan area is too small prior to 50 h), and for the aggradation phase between 100 and 160 h. An unavoidable consequence of this is that the aggradation data set is six times larger than the progradation series. To locate a characteristic time, we fit a best fit exponential curve to the data of the form $C = ae^{-\beta t} + c$, where parameter β tracks the rate of decorrelation, c gives the asymptotic correlation and is zero if the system is unconfined and therefore able to become completely uncorrelated, and a is approximately $1 - c$ [*Wickert*, 2007]. For consistency with the shoreline time scale (discussed in detail below), we characterize the channel decorrelation time T_{ch} as the point at which roughly 95% of the total channel decorrelation occurs.

[20] Channel decorrelation results are shown in Figures 3a and 3b, where we identify two features worthy of note. First, the exponential regressions do not asymptote at zero, but rather at 0.13 (progradation) and 0.14 (aggradation), highlighting that the fan surface does not completely decorrelate with itself. It turns out here that local correlation is a natural and desired outcome of the experimental set up, where the inlet channel geometry continued onto the proximal fan surface for much of the experiment and acted as the input channel for the distributary system. Second, $T_{\mathrm{ch,prog}}$ is 23.5 h whereas $T_{\mathrm{ch,agg}}$ is 12.5 h, demonstrating that on average channel mobility, which could be considered avulsion frequency of the form $f_A = 1/T_{\mathrm{ch}}$, increased by a factor of 1.9 in response to equilibrium base-level rise.

5.2. Channel Mobility and Deposition

[21] In order to test the apparent link between channel mobility and net deposition (both increase by a factor of about 2), we derive a dimensionless aggradation parameter, h_*, given as

$$h_*(x,y) = \left[h_{\mathrm{agg}}(x,y)/h_{\mathrm{ch}}\right] = \left\{\left[\int_0^{T_{\mathrm{ch}}} \dot{\eta}(x,y)dt\right] \Big/ h_{\mathrm{ch}}\right\}, \quad (3)$$

where h_{agg} is the accumulated depositional thickness over time scale T_{ch} (the time integral of measured aggradation rate $\dot{\eta}$), and h_{ch} is a characteristic channel depth of 5 mm determined from direct measurement. Parameter h_* is similar to (but does not replicate) dimensionless aggradation as defined by *Mohrig et al.* [2000], who also referenced accumulated channel aggradation thickness to flow depth from ancient channel fill deposits; the key differences are that here (1) h_* is measured across the fluvial surface and is not limited to channel positions, (2) we use one representative channel flow depth, and (3) we are therefore unable to couple local flow depth with adjacent local aggradation thickness data. Frequency distributions for h_*, referenced to the channel time scales, are shown in Figure 3b and exhibit strong similarity for $h_* \geq 0.8$. (For $h_* < 0.8$ the distributions diverge, a likely consequence of increased wetted area during the phase of equilibrium base-level rise, an interesting result left for future work). In fact, despite a twofold change in channel mobility the average values for h_* are similar: $\overline{h}_{*,prog} = 1.08$ and $\overline{h}_{*,agg} = 0.90$, indicating that the loss in channel pattern is driven by deposition that on average creates differential topography of about one channel depth. These results are similar to field measurements [*Mohrig et al.*, 2000], although relatively greater variability exists in the experimental case because of points 1–3 above. The positive correlation between net deposition and channel mobility found here is qualitatively similar to the avulsion response for alluvial fan delta and braided river environments [*Bryant et al.*, 1995; *Ashworth et al.*, 2004], indicating the relationship between deposition and channel migration is at least broadly insensitive to environment.

[22] The mechanisms leading to avulsion in DB07, however, are rather poorly understood and may not be completely related to gradual channel alluviation [e.g., *Tornqvist and Bridge*, 2002; *Slingerland and Smith*, 2004]. Rather, in DB07 we observe channel network migration to be driven by upstream-migrating sedimentation waves that backfill channels and originate at the shoreline as hydraulic instabilities [*Hoyal and Sheets*, 2009]. Deposition is driven in part by flow expansion that bears some similarities to depositional flow patterns in noncohesive braided distributary systems [*Sheets et al.*, 2002] and sedimentation processes inferred from ancient turbidite deposits [*Gardner and Borer*, 2000].

6. Persistence of Shoreline Regression

[23] Our attempt to link channel and shoreline kinematics is based on the well-founded notion that the shoreline is an important boundary in fluviodeltaic environments that is responsive to upstream channel-related process controls [*Swenson et al.*, 2000]. For example, *Kim et al.* [2006] have shown that the shoreline response to autogenic channel dynamics can be long-lived and capture different frequencies of fluvial processes. In DB07 distributary lobe development and associated migration of the shoreline is a qualitative indication that the shoreline is sensitive to the channel network, and consequently should respond to channel migration. Here we examine the link between the shoreline and channel kinematics by performing an independent analysis of shoreline persistence, with the goal of developing a shoreline time scale that can be compared to the channel time scale above.

6.1. Shoreline Structure

[24] The shoreline is a contour of the delta surface and in DB07 forms a complex boundary that spans an angular distance of roughly 120° (Figure 4a). We characterize the shoreline using polar coordinates, where for each angular position θ measured with respect to the delta inlet there is

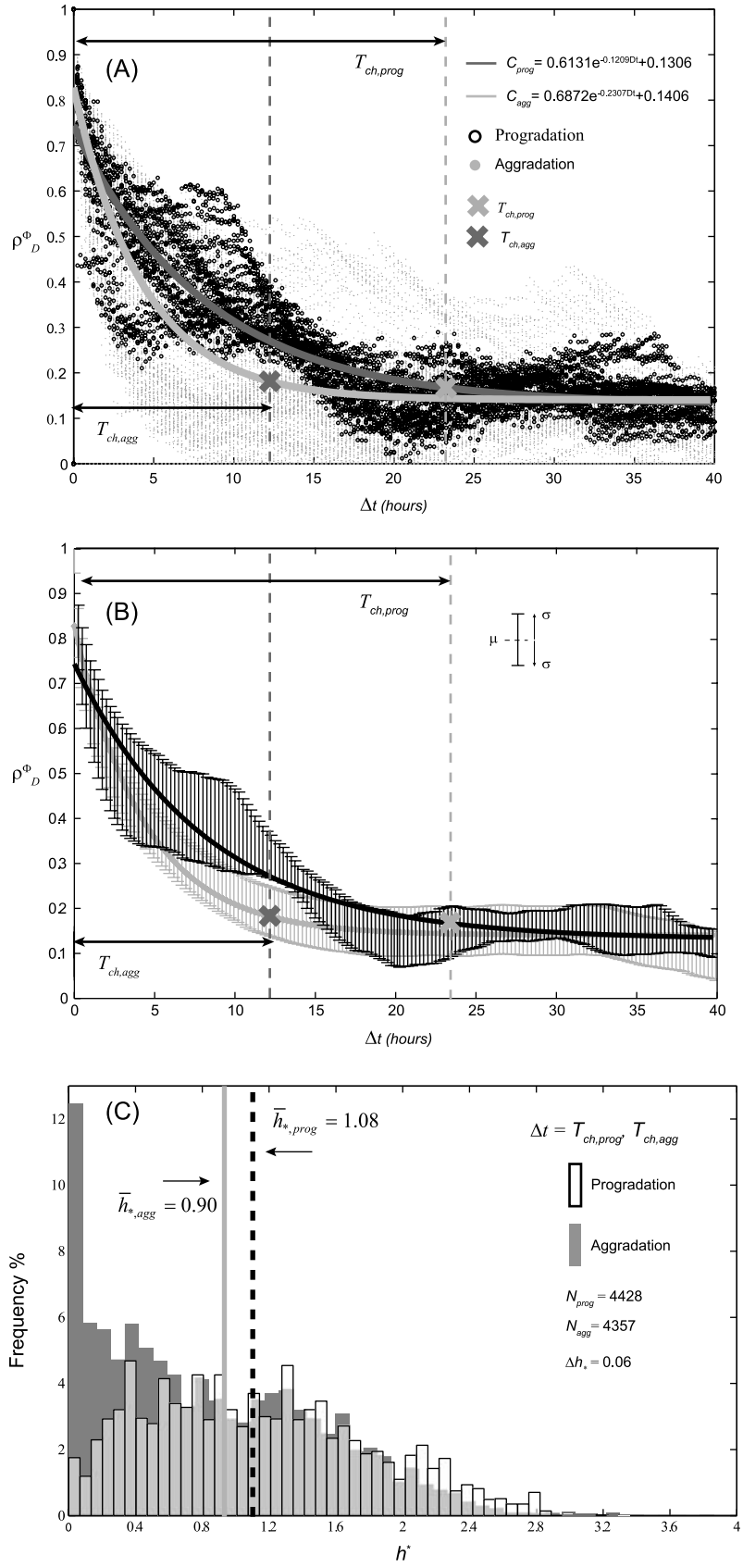

Figure 3. (a) Channel decorrelation for progradation and aggradation phases of the experiment. (b) Error plot showing ±1 standard deviation from the mean channel decorrelation value superimposed on best fit exponential decay curves. (c) Histogram of h_* for appropriate time scales, $T_{\mathrm{ch,prog}}$ and $T_{\mathrm{ch,agg}}$.

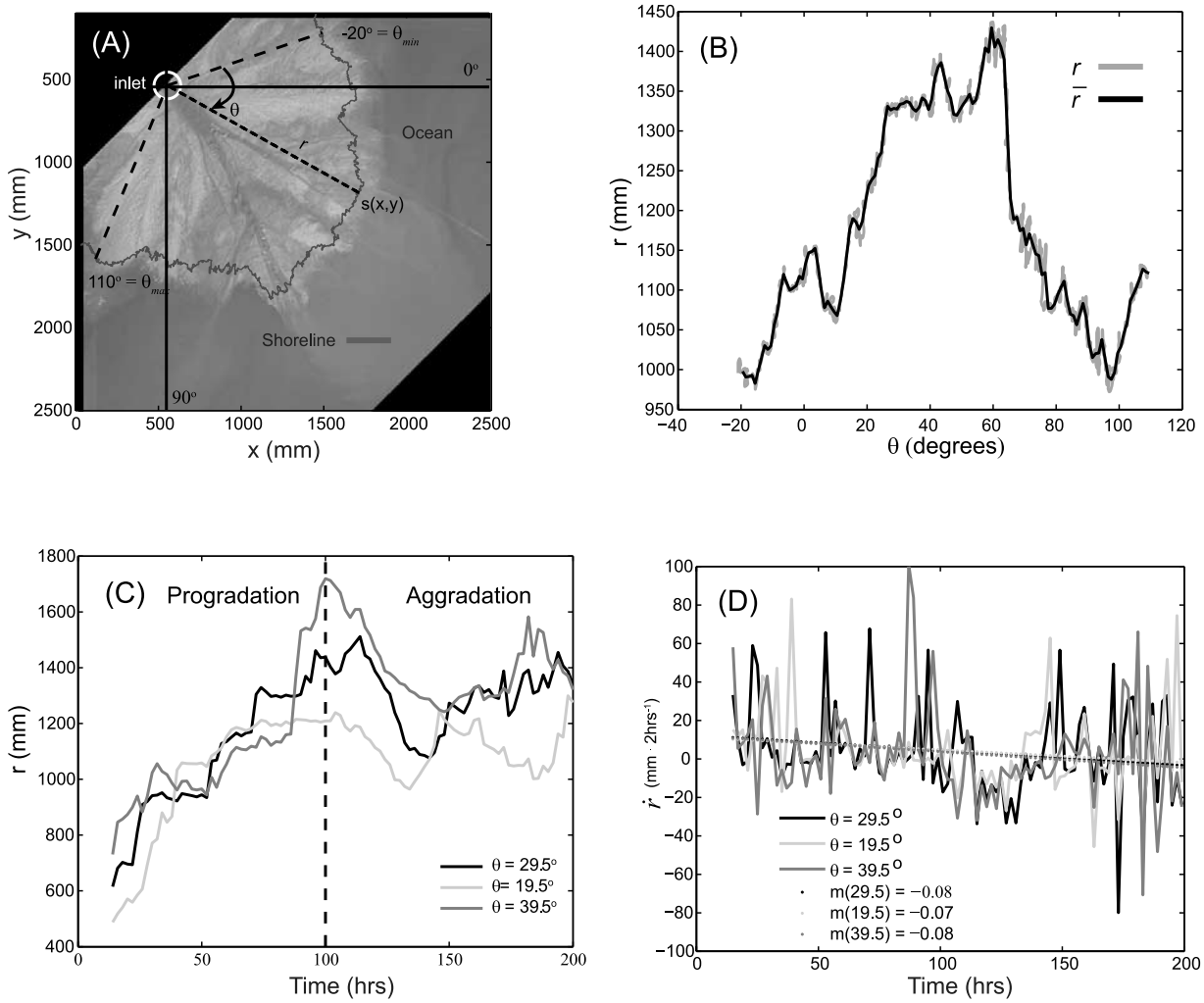

Figure 4. (a) Graphical relationship between shoreline measured in Cartesian ($s(x, y)$) and polar ($s(r, \theta)$) coordinates. (b) Original and averaged shoreline profile in polar coordinates. (c) Shoreline radius with time illustrating nonstationarity. (d) Shoreline migration rate $\dot{r}$ is approximately stationary as noted by the small slope (m) values from a linear regression of the data.

one or more associated radial distance to the shoreline r, depending on $\Delta\theta$ and the local shoreline rugosity (Figure 4b). For this analysis it is convenient to have one r value for each θ, requiring us to average distance locally such that $r = \bar{r}$. We note that one issue with the r, θ method is that the amount of averaging required is a function of the fluvial length at a given θ. However, by comparing the resolution of averaged data against the original, we find that $\Delta\theta = 1^\circ$ is a sufficiently narrow window to provide excellent data fidelity and minimize averaging effects (Figure 4b).

[25] At an arbitrary θ the shoreline time series $r(\theta, t)$ in DB07 is considered nonstationary because it does not have a constant mean. This is due to background fan growth during progradation (deterministic nonstationarity) and variable growth and retraction during fan aggradation (stochastic nonstationarity) (Figure 4c). We remove most of these trends by using shoreline migration rate $\dot{r}(\theta)$ (i.e., the time derivative of shoreline position, $\dot{r}(\theta) = \partial r(\theta)/\partial t$), which is equivalent to a first-order difference technique to create stationarity [*Box and Jenkins*, 1976] (Figure 4d). (Weak nonstationarity in $\dot{r}$ is still present during delta progradation because the average shoreline regression rate must slow over time as the topset depositional area increases.)

6.2. Shoreline Regression

[26] With the transformed data we are able to visualize shoreline kinematics by generating a time structure map of shoreline regression against θ and against time t (i.e., $\dot{r}(\theta, t)$ for $\dot{r} \geq 0$). Given the significant range of $\dot{r}$ we display it by its natural logarithm $\dot{r}_{\ln}$ (Figure 5a). The map is limited to $\dot{r} \geq 0$ because of our assumption that the persistence of shoreline *regression* is the key link to the channel network. We observe differences in the configuration of shoreline regression between delta progradation and aggradation, where coherent structures present during progradation appear to lose time and space correlation during fan aggradation (Figure 5a). Additionally, very small shoreline regression rates apparent in the structure map during fan progradation disappear after the onset of base-level rise, highlighting the fact that after this point in time a larger shoreline sediment flux is required for shoreline regression.

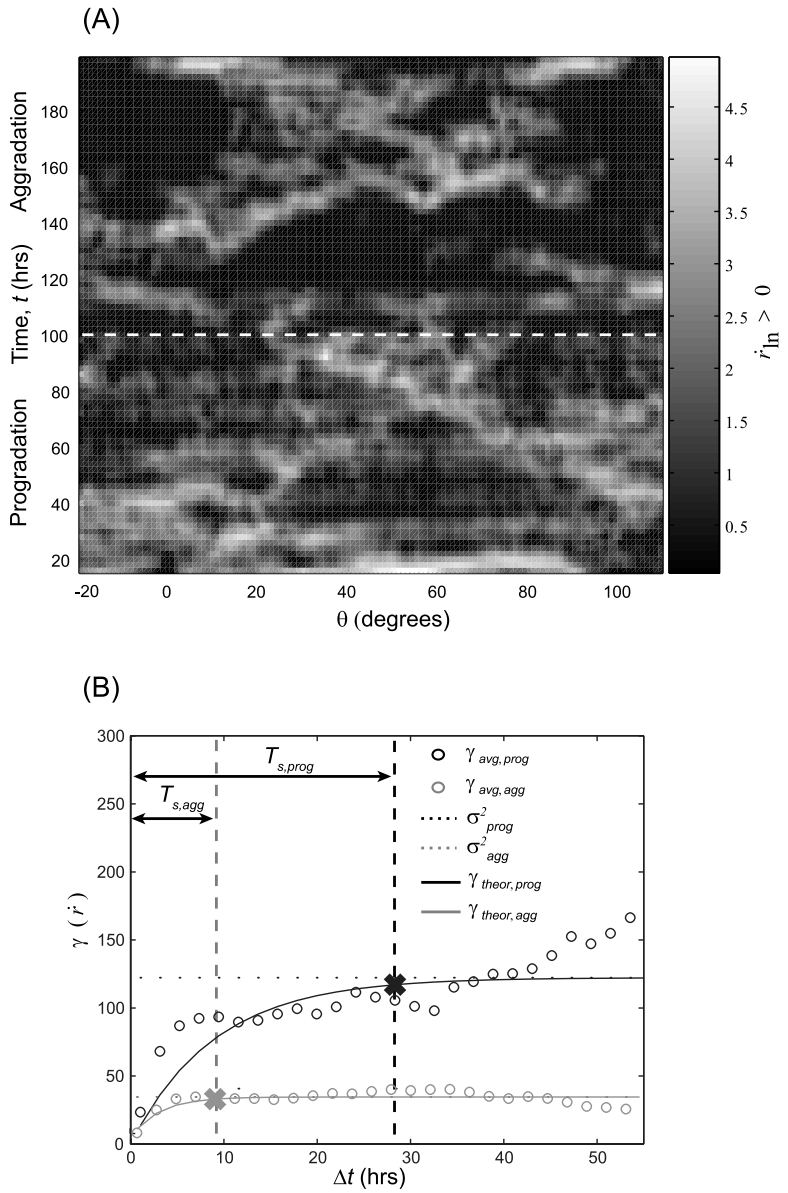

Figure 5. (a) Time structure map of shoreline regression rate $\dot{r}_{\ln}$. (b) Time directional variograms for the progradation and aggradation phases of DB07. Asymptotic deviation away from the theoretical sill in the progradation phase variogram results from long-term decreases in the shoreline regression rate. This effect is due to an expanding topset depositional area during delta progradation.

6.3. Shoreline Time Scale

[27] We quantify a shoreline time scale by treating $\dot{r}$ as a stochastic process and express its structure through use of a variogram, defined by

$$\gamma(h) = (1/2)\left\{[\dot{r}(\underline{x}_1) - \dot{r}(\underline{x}_2)]^2\right\}, \quad (4)$$

where $\underline{x}_k$ is a position in the domain $\boldsymbol{t}$, $\boldsymbol{\theta}$ ($t_0 \le \boldsymbol{t} \le t_{max}$ and $\theta_0 \le \boldsymbol{\theta} \le \theta_{max}$) and h is a "distance" between two positions (i.e., $h = \underline{x}_1 - \underline{x}_2$). By using $\dot{r}$ we assume approximate stationarity of the process and that the variance of $\dot{r}$ is primarily a function of h. Here we are specifically interested in time changes, i.e., $\gamma(\Delta t)$, such that (4) can be rewritten as

$$\gamma(\Delta t) = (1/2)\left\{[\dot{r}(\theta, t) - \dot{r}(\theta, t + \Delta t)]^2\right\}. \quad (5)$$

It is obvious that when $\Delta t = 0$, $\gamma(0) = 0$. As Δt increases we expect $\gamma(\Delta t)$ to increase as well since $\dot{r}(t)$ and $\dot{r}(t + \Delta t)$ are more likely to have different values. Variability cannot increase without bound, however, and beyond some characteristic Δt_{char}, $\gamma(\Delta t_{char})$ plateaus at the variability of the data, $\sigma^2_{\dot{r}}$, i.e., $\gamma(\Delta t_{char}) \cong \sigma^2_{\dot{r}}$. We define the characteristic shoreline time scale Δt_{char} as T_s, where specifically $\gamma(T_s) = 0.95\sigma^2_{\dot{r}}$. T_s then represents the largest, or dominant time scale over which two values of $\dot{r}$ are correlated.

[28] In order to most accurately link the channel network with shoreline regression, we target the time persistence of shoreline regression, i.e., $\dot{r} > 0$, since locally shoreline accretion basinward implies a sediment source from a channel conduit. Thus, in this analysis at the ith time t and jth position θ we impose the following restriction in (4): $\dot{r}(\theta_j, t_i) > 0$.

[29] Time directional variograms for the progradation and aggradation phases of DB07 are shown in Figure 5b. An exponential model fit to the data shows that $T_{s,\mathrm{prog}}$ is 28.3 h and $T_{s,\mathrm{agg}}$ is 9.5 h. We note that these values are meaningful when overlain on the time structure map $\dot{r}(\theta, t_i)$, where they approximate the correlation lengths one might draw from observations alone. Also, by characterizing the channel network and shoreline, two related but dynamically distinct quantities, by the average time separation between two points corresponding to 95% correlation loss, their respective time scales are reasonably close: $T_{\mathrm{ch,prog}}/T_{s,\mathrm{prog}} = 0.8$ and $T_{\mathrm{ch,agg}}/T_{s,\mathrm{agg}} = 1.3$, confirmation that increased channel mobility is directly translated to the shoreline as a decrease in the time persistence of regression at an arbitrary θ location.

6.4. Implication of T_s for Shoreline Dynamics

[30] It is worth stating here that T_{ch} and T_s reflect the largest scale of autogenic delta mobility. Superimposed on this is a large amount of local, high-frequency variability, which presumably signals similar local irregularity in channel processes near the fan fringe (Figure 5a). *Hoyal and Sheets* [2009] have equated rapid local shoreline regression with elongating pioneering channels. Flow instability within the channel eventually forces flow bifurcations and the creation of additional channels. The fact that T_s is much larger than these fluctuations and is associated with T_{ch}, which characterizes an "avulsion" time scale, supports the idea of additional surface instabilities [*Jerolmack and Swenson*, 2007]. For example, on relatively short time scales in-channel instabilities force flow spreading and the formation of multiple bifurcation-based channels [*Edmonds and Slingerland*, 2007], and on longer time scales (e.g., T_{ch}, T_s) another instability arises from differential topography, causing larger-scale shifts in the flow [*Jerolmack and Mohrig*, 2007; *Jerolmack and Swenson*, 2007]. The implication for distributary lobes in DB07 is that the site of lobe evolution may be established by fan topography, whereas the details of lobe growth are accomplished by a subset network of bifurcation channels that stem from a parent channel. In this view, the Wax Lake Delta, which is composed of a similar network of bifurcating channels, is more equivalent to a distributary lobe in DB07 than the entire composite deltaic body (Figure 2c).

7. Shoreline Scaling Properties and Their Interpretation

[31] We demonstrated in section 6.4 that persistence of shoreline regression is sensitive to channel processes through a close association between T_{ch} and T_s. This provides some support for the notion that shoreline geometry may also be responsive to important kinematic properties of fan delta organization in DB07. Shoreline contours exhibit roughness elements stemming from single channels and lobes, both of which are constantly evolving features and variably expressed in the shoreline contour. Consequently, identifying such features in the shoreline profile is tedious and subjective. Rather, we continue our treatment of the shoreline as a random variable and its inherent spatial variability is treated as a roughness, which has been successfully incorporated for bed forms [*Nikora et al.*, 1997; *Jerolmack and Mohrig*, 2005]. A commonly used roughness metric is the root mean squared deviation of the feature of interest, here the shoreline distance r, defined by

$$w = \left[(1/N) \sum_{i=1}^{N} \left(r_{d,i} - \overline{r}_d \right)^2 \right]^{1/2}, \tag{6}$$

where r_d is the detrended shoreline radius to a best fit polynomial in order to remove the asymmetry in the delta planform, $\overline{r}_d$ is the mean detrended shoreline distance over the $\Delta\theta$ considered, and N is the total number of measurements, also dependent on $\Delta\theta$. w is referred to as the interface width by *Barabasi and Stanley* [1995], and refers to the variability (measured as a length) in r_d as a function of window size $\Delta\theta$. Over some range the scaling of w with $\Delta\theta$ is often of the form

$$w \sim \Delta\theta^{\alpha}, \tag{7}$$

where α is the roughness exponent. In the case of DB07, the smallest $\Delta\theta$ is 1°, which is at the data resolution used in the analysis. We then take the average of all w values to obtain a characteristic roughness for that $\Delta\theta$. The process is repeated with progressive increases in window size (by 1° increments) up to a maximum $\Delta\theta$ of 80°, 75% of the total angular span of the shoreline used in the analysis (Figure 6).

[32] The characteristic interface width w plotted against $\Delta\theta$ for progradation and aggradation shoreline data show several key features (Figure 6). First, we identify a lower-scale invariant regime in which a scaling relationship holds between w and $\Delta\theta$, where the roughness exponent α is the slope of the line. Second, as the window size increases we observe a gradual break from the power law relationship as the curve rolls over to approximately horizontal, indicating a saturation in roughness despite increases in $\Delta\theta$. Third, the characteristic growth exponent α, transition crossover angle $\Delta\theta_x$, and interface width w_x, are similar despite differences in the dominant delta time scales quantified above (Figure 6). And lastly, though α is constant, some variability exists in $w(\Delta\theta)$ (coefficient of variation is ~20%).

[33] Taken together, the shoreline data are robustly characterized by saturation in roughness at $\Delta\theta_x = 16.5°$. This occurs well below the maximum angle window used, indicating delta organization that limits the wavelength of shoreline fluctuations. By projecting $\Delta\theta_x$ onto the fan planform, we find that it is proportional to the observed angular span of distributary lobes $\Delta\theta_L$ as $2\Delta\theta_{\mathrm{x}} \sim \Delta\theta_L$ (Figure 7). The associated saturation interface width is w_x = 62.5 mm. By averaging the upper one-fourth of Δr (the average fractional angular span of delta lobes) over $\Delta\theta_x$ we derive a characteristic distributary lobe length scale L_L for DB07 of about 220 mm. Variability in $w(\Delta\theta)$ is modulated dynamically by the sediment flux at the shoreline and

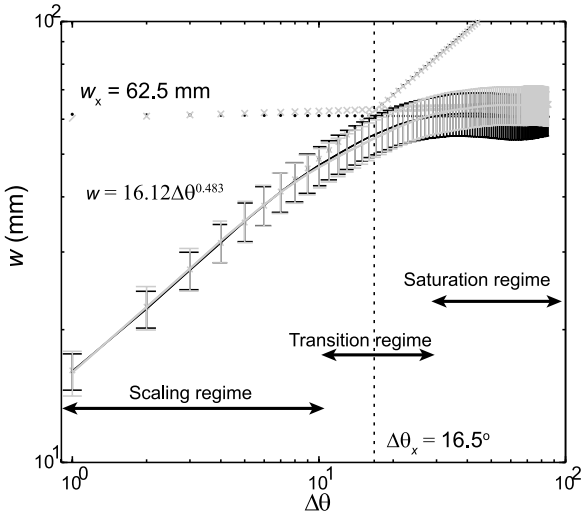

Figure 6. Averaged shoreline scaling results from DB07. Note that no significant differences exist in statistical shoreline geometry between fan progradation (black) and aggradation (gray). Error bars represent 1 standard deviation of roughness (w) for a given angular window ($\Delta\theta$).

geometrically by the background shape of the shoreline from which lobe progradation occurs [*Hoyal and Sheets*, 2009]. Sediment bypass at the shoreline is largely established by the degree of channelization on the fan surface, where we expect that increased flow focusing will lead to greater local flux and consequently larger protrusions in the shoreline. By plotting a time series of $w_x(t)$ against the fluvial wetted fraction $f_w(t)$ we find that on average this is the case, where a negative correlation is derived ($\rho(w_x(t), f_w(t)) = -0.3$). The instantaneous shoreline geometry at the onset of distributary lobe growth is also important. For example, if the shoreline is initially very smooth then lobe growth will increase $w(\Delta\theta, t)$; however, if lobe growth is filling in a local reentrant in the shoreline then $w(\Delta\theta, t)$ will decrease. Consequently, noisy growth and dissipation of shoreline roughness around a characteristic w_x is an intrinsic outcome of the migration of distributary lobes.

[34] Growth in shoreline variability with increasing $\Delta\theta$ up to one-half the angular span of distributary lobes, the largest self-formed fan delta features reflected in the shoreline, occurs by the power law relationship above. Similar results from shoreline power spectra implies a continuum of variability in r where no characteristic sublobe-scale features can be identified [*Barabasi and Stanley*, 1995]. Thus, the distinction of the smaller channel, or "jet," length scale of *Hoyal and Sheets* [2009], while an important element in fan delta morphodynamics, is not apparent in the shoreline. This suggests to us that distributary lobes are created through the relatively rapid creation, splitting, and amalgamation of bifurcation channels [e.g., *Edmonds and Slingerland*, 2007] and linked offshore deposits in which the associated local shoreline protrusion has no characteristic length, creating the observed scale invariance in the shoreline. The local sediment transport dynamics that maintain the scaling regime are interpreted to be rapid because fluctuations in r increase with identical growth exponents during fan progradation and

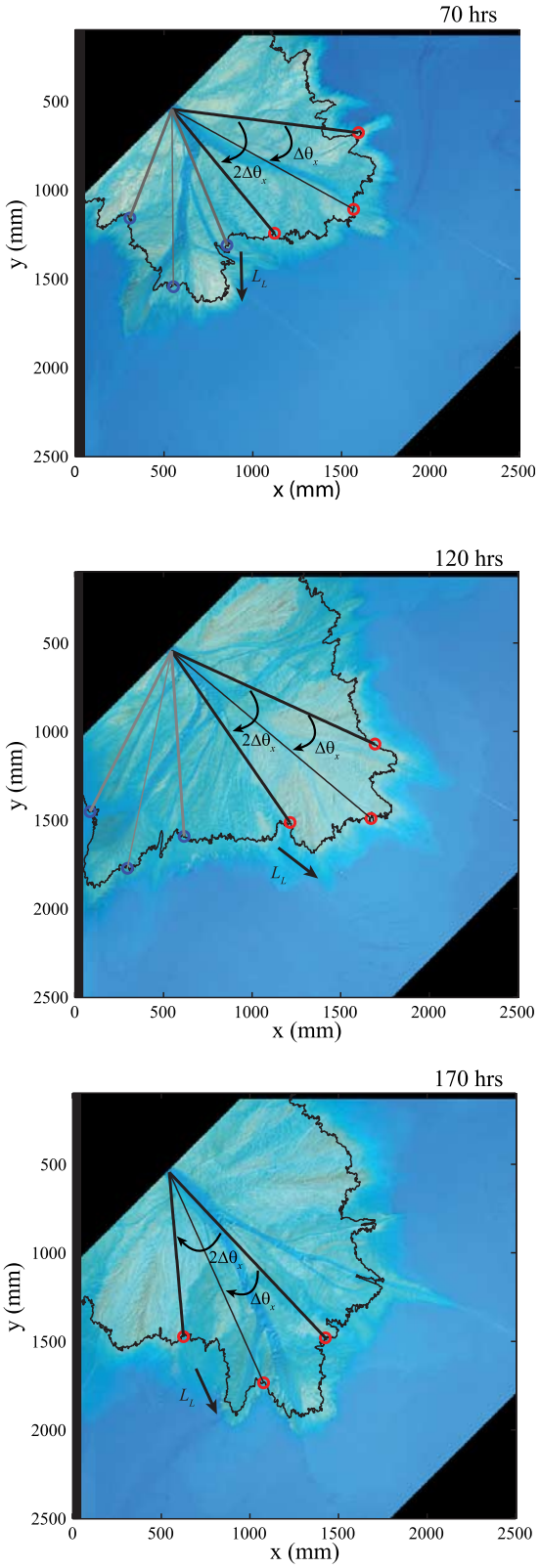

Figure 7. Three images illustrating the projection of the angular span at which shoreline roughness saturates, $\Delta\theta_x$, onto the delta surface. By multiplying this value by 2 we recover the average angular span of interpreted distributary lobes.

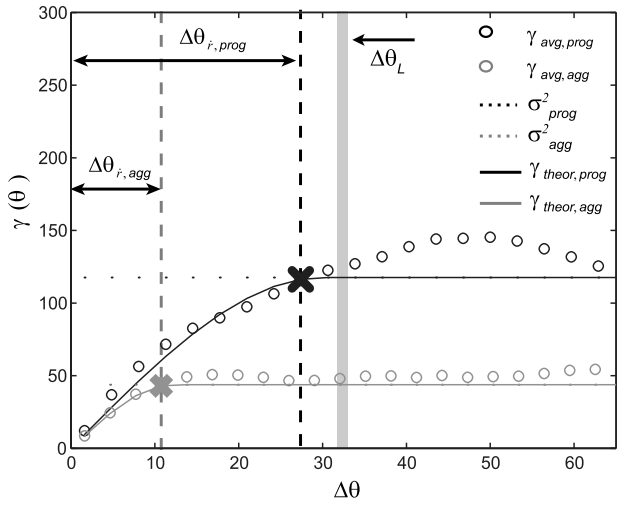

Figure 8. Directional variograms (in space) for the progradation and aggradation phases of DB07.

aggradation (Figure 6), despite significant differences in the characteristic delta time scales.

8. Coupling Delta Kinematics With Spatial Scaling of the Shoreline

8.1. Shoreline Structure and Delta Process Coupling During Progradation

[35] We find evidence for a direct association between surface kinematics and shoreline geometry during delta progradation. The strongest support for this is derived from spatial correlation analysis of shoreline regression $\dot{r}$. Recall that above we use a directional variogram $\gamma(\Delta t)$ to estimate shoreline time persistence. By measuring the lateral correlation length of shoreline regression $\gamma(\Delta\theta)$

$$\gamma(\Delta\theta) = (1/2)\left\{[\dot{r}(\theta,t) - \dot{r}(\theta+\Delta\theta,t)]^2\right\}, \quad (8)$$

we generate a characteristic $\Delta\theta$, $\Delta\theta_{\dot{r}}$, that can be directly compared to $\Delta\theta_x$. During delta progradation $\Delta\theta_{\dot{r},prog}$ is 27°, a close match to the characteristic distributary lobe angular span derived from spatial analysis of the shoreline, where $2\Delta\theta_x = \Delta\theta_L = 33°$ (Figure 8). That is, during progradation expansion of the fan delta occurs over a characteristic angular window that we observe as distributary lobes. Consequently, shoreline regression is directly imprinted on the shoreline scaling. A second line of evidence that points to this coupling is that the derived averaged quantities agree. By averaging $\dot{r} > 0$ over the progradation stage of the experiment and multiplying it by $T_{s,\mathrm{prog}}$ we derive a regression length scale $L_{R,\mathrm{prog}}$ of 203 mm, which closely matches the distributary lobe length scale L_L of 220 mm independently measured from the shoreline scaling analysis.

8.2. Shoreline Structure and Delta Process Decoupling During Aggradation

[36] The shoreline maintains a robust statistical steady state despite significant increases in surface kinematics after the onset of equilibrium base-level rise (Figure 6). This result differs from our expectation that w_x, and thereby $\Delta\theta_x$ and L_L, should be significantly reduced during aggradation (i.e., the shoreline should be much smoother) owing to the increase in delta mobility, where $T_{\mathrm{ch,agg}}/T_{\mathrm{ch,prog}} = 0.51$ and $T_{s,\mathrm{agg}}/T_{s,\mathrm{prog}} = 0.34$. Constant shoreline scaling between fan progradation and aggradation quantitatively shown in Figure 6, however, is also visually apparent to us, where in a random sampling of shorelines (not shown) we cannot readily distinguish them on the basis of the experiment stage. This highlights an intriguing disassociation between delta kinematics (i.e., T_{ch}, T_s) and shoreline geometry (i.e., $\Delta\theta_x$, w_x) during fan aggradation. For example, here the derived average kinematic and geometric quantities disagree, where the averaged $\dot{r} > 0$ multiplied by $T_{s,\mathrm{agg}}$ results in a regression length scale $L_{R,\mathrm{agg}}$ of 102 mm, roughly one-half of what is measured from the shoreline directly (i.e., $L_{R,\mathrm{agg}}/L_L = 0.46$). Moreover, during fan aggradation $\Delta\theta_{\dot{r}}$ contracts to 11°, presenting a similar departure between the characteristic angular span of shoreline regression and distributary lobes measured from the shoreline (i.e., $\theta_{\dot{r},agg}/\theta_L = 0.33$) (Figure 8). We briefly explore two possible resolutions to this issue, one that actually preserves the kinematic-geometric association, and one in which a disconnection is maintained.

8.3. Interpretation of Geometric-Kinematic Decoupling

[37] One possible explanation is that base-level rise and transgression over inactive portions of the fan surface set up a condition for shallow flooding followed by rapid local delta progradation. In this case the growth of distributary lobes simply occurs much faster. Measurements of average positive shoreline migration $\bar{\dot{r}}$ are 8.6 mm h^{-1} and 10.7 mm h^{-1} during fan progradation and aggradation, respectively, too similar to cause significant differences in distributary lobe growth. Further, histograms of $\dot{r}$ (not shown) exhibit similar tail distributions, suggesting that the frequency of relatively fast shoreline regression is not significantly greater during fan aggradation.

[38] An alternative is that shoreline transgression during base-level rise largely compensates for the delta's inability to maintain its previous level of shoreline roughness during progradation. For example, if greater mobility of the delta system acts to smooth the shoreline, one buffer to this effect is relative base-level rise, which by forcing transgression over inactive areas of the delta statistically maintains shoreline roughness. This possibility is demonstrated by a simple geometric estimation of shoreline transgression over $T_{s,\mathrm{agg}}$, where we derive a transgression length as $L_{T,\mathrm{agg}} = \omega T_{s,\mathrm{agg}}/S_A$ equal to 89 mm. This value, when combined with $L_{R,\mathrm{agg}}$ leads to a total length of 191 mm (i.e., $L_{T,\mathrm{agg}} + L_{R,\mathrm{agg}} = 191$ mm), closer to the distributary lobe length scale L_L of 220 mm.

[39] Further, shoreline transgression is the only physically plausible underlying cause in reducing $\Delta\theta_{\dot{r}}$ by a factor of one-third during fan aggradation. This mechanism is supported by the results above that show the increase in delta aggradation and decrease in $\Delta\theta_{\dot{r}}$ are by nearly the same amount (between a factor of 2 and 3), implying that the base-level rise effect on delta aggradation is approximately linearly translated to shoreline transgression though the fluvial slope. Consequently, the similarity between $\dot{\eta}_{\mathrm{agg}}/\dot{\eta}_{\mathrm{prog}} = 1.91$ and both $T_{s,\mathrm{prog}}/T_{s,\mathrm{agg}} = 3.0$

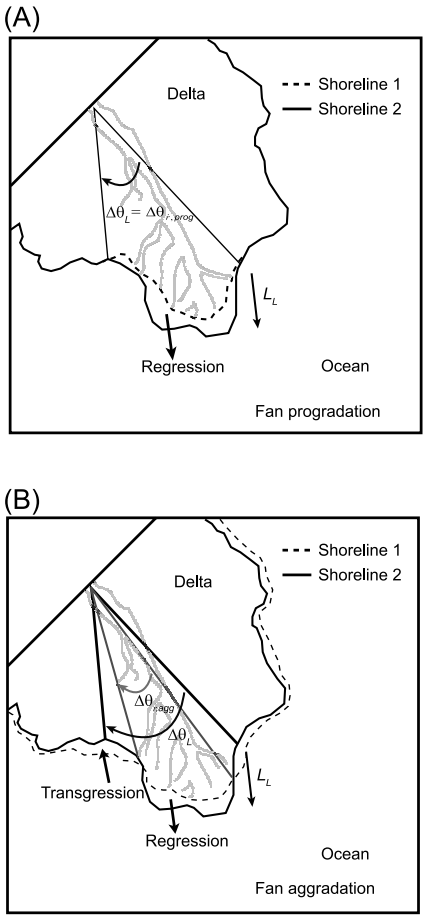

Figure 9. Schematic diagram of the coupling and partial decoupling of fan processes and shoreline geometry. (a) During fan progradation, all shoreline roughness is constructed by fan processes, forming a correspondence between shoreline regression (captured in $\Delta\theta_{\dot{r}}$) and shoreline geometry (captured in $\Delta\theta_L$). (b) During fan aggradation, shoreline geometry is only partially set by fan processes, being complemented by shoreline transgression over inactive portions of the delta, thus, $\Delta\theta_{\dot{r}} \neq \Delta\theta_L$.

and $T_{ch,prog}/T_{ch,agg} = 1.88$ suggests that the effect of relative base-level rise on shoreline transgression is evenly matched to the increased mobility of delta lobe migration (Figure 9).

9. Discussion

[40] The generation of characteristic time and space scales seems to provide a relatively robust method to describe and evaluate stochastic autogenic processes. Moreover, if guided by theoretical insight and applied in dimensionless form there is no reason their expected correlations cannot be tested against natural systems and numerical models. DB07 provides a first look into how the averaged kinematics of a well-channelized delta responds to equilibrium base-level rise in the form of two time scales, T_{ch} and T_s, and modulates shoreline geometry. The apparent decoupling of time and space scales during equilibrium base-level rise and fan aggradation has stimulated us to consider further how common this effect might be. In the case of DB07, the balancing act between fan delta mobility and relative base-level rise in maintaining a steady state shoreline geometry is supported by the fact that both vary by similar amounts. At this point we are unable to assess whether this is a natural outcome of equilibrium base-level rise because this experiment represents one data point. However, using the geometric relations for fan aggradation given in (1) and (2) together with a theoretical avulsion time scale proposed by *Jerolmack and Mohrig* [2007]

$$T_{ch,theor} = h_{ch}/\dot{\eta}, \tag{9}$$

we derive a $T_{ch,prog}$ of 22.6 h and $T_{ch,agg}$ of 12.3 h, close to the empirical measurements. In (9) the relation between fan delta mobility and fan aggradation is made explicit, and therefore $T_{ch,prog}/T_{chs,agg}$ will always be proportional to $\dot{\eta}_{agg}/\dot{\eta}_{prog}$ in the dynamic range between absolute fan progradation and aggradation. The implication from this is that, in the absence of offshore reworking, shoreline geometry is statistically maintained. This predicts that, for example, the dominant shoreline length scale L_L is largely constant and independent of the average shoreline trajectory.

[41] Decoupling of fan processes and shoreline geometry leads us to consider another potential decoupling between fan delta kinematics and internal stratigraphy. While we leave the details of the experimental stratigraphy to a later study, mechanistic considerations of avulsions imply three classes of stratigraphic organization based on the response of avulsion frequency to net aggradation [*Bryant et al.*, 1995; *Heller and Paola*, 1996]. One predicted end-member stratal arrangement is remarkable insofar as it does not signal changes in avulsion frequency and results from a linear relationship between avulsion and aggradation. The results we observe for the experimental delta are analogous to this case, in that the increased production of channels is largely matched by storage capacity. It is worth pointing out that at smaller (e.g., channel) scales, such stratigraphic insensitivity to aggradation has been demonstrated both experimentally and in the field for braided alluvial channels [*Ashworth et al.*, 1999].

[42] A less appreciated and understood element of this that has direct bearing on the deposit architecture is the effect of delta aggradation on surface geomorphology, such as the number, size, and branching geometry of active channels [*Tornqvist*, 1994]. *Jerolmack and Mohrig* [2007] have demonstrated that channel coexistence can be broadly categorized on the basis of comparing channel migration versus aggradation time scales. One drawback to our analysis of channel decorrelation is that it is insensitive to the style of mobility, and we acknowledge that its influence on alluvial architecture is important, since, for example, for fluid conservation a greater number of active channels must result in a smaller average channel cross-sectional area. Beyond continued development of algorithms to describe surface channel geometry and networks [e.g., *Fagherazzi et al.*, 1999], which may help in further quantifying various channel types and their kinematics [e.g., *Edmonds and Slingerland*, 2007], another major challenge is the channel burial process [e.g., *Sheets et al.*, 2007], which inevitably must transform geomorphic channels to stratigraphic channel fill deposits. This general line of investigation may bear fruit for the oil industry, where quantification of channel

fill geometry and channel thread connectedness is only beginning. Outstanding questions in this respect are: (1) the extent to which burial processes remove the bounding geometry of fossilized channel fills from their previous surface configuration, with special attention to preserved channel lengths; and (2) the degree to which the distribution of fossilized channel fill structures statistically honors the geometry of the surface sediment transport system, which could be attempted through formal scaling of the surface and (if possible) buried channel network structure.

10. Conclusions

[43] Our conclusions are as follows:

[44] 1. An initial experiment with a new, weakly cohesive sediment mix shows that the cohesive material leads to delta morphology that shows a greater degree of bifurcation and a wider range of shoreline roughness scales than comparable experiments with noncohesive sediment.

[45] 2. The advent and continuation of steady, equilibrium base-level rise shifts the sediment mass balance to greater alluvial sediment storage by increasing fluvial accommodation. In this example, the delta surface aggradation rate increased by a factor of roughly 2 after the onset of base-level rise. Increased net deposition modified two important and closely related geomorphic time scales, T_{ch} and T_s, which characterize channel and shoreline kinematics, respectively.

[46] 3. Between the progradation and aggradation phases of the experiment, T_{ch} decreased by a factor of about 2, and T_s was reduced by a factor of 3. These are proportional to the factor of increase in the average surface aggradation rate of approximately 2. These results demonstrate a close dynamic linkage between the fluvial transport system and the shoreline, and an approximately linear affect of increased deposition on delta topset kinematics.

[47] 4. Spatial analysis of the shoreline reveals a lower-scale invariant regime where shoreline roughness grows as a function of length, $\Delta\theta$, and an upper saturation regime where shoreline roughness is independent of $\Delta\theta$. The transition between the two, $\Delta\theta_x$, is proportional to the angular span of individual distributary lobes $\Delta\theta_L$ (i.e., $2\Delta\theta_x \sim \Delta\theta_L$), indicating that distributary lobes are the largest roughness elements expressed in the shoreline.

[48] 5. Shoreline geometry, as measured through its scaling properties is independent of the experiment phase and exposes a coupling between fan kinematics and shoreline geometry during fan progradation, and a decoupling during fan aggradation. Throughout progradation shoreline geometry is a direct reflection of fan expansion into the basin through the growth of distributary lobes. However, during aggradation shoreline is created by distributary lobe growth *and* shoreline transgression over inactive portions of the fan.

[49] **Acknowledgments.** We thank ExxonMobil Research Company for financial support and, in particular, Kevin Barnes for his stewardship of this project. We are indebted to John Swenson, Doug Jerolmack, Matt Wolinsky, and Stephanie Day for stimulating discussion and to Jim Mullin, Chris Ellis, Dick Christopher, and Craig Hill for their expertise in building and recording experimental landscapes. Reviews by Rudy Slingerland, Doug Jerolmack, and an anonymous reviewer helped in clarifying our results and are greatly appreciated.

References

Alexander, J., and M. R. Leeder (1987), Active tectonic control on alluvial architecture, in *Recent Developments in Fluvial Sedimentology*, *Soc. Econ. Paleontol. Mineral. Spec. Publ. Ser.*, vol. 39, edited by F. G. Ethridge, R. M. Flores, and M. D. Harvey, pp. 243–252, Soc. of Econ. Paleontol. and Mineral., Tulsa, Okla.

Ashmore, P. E. (1991), How do gravel-bed rivers braid?, *Can. J. Earth Sci.*, *28*, 326–341.

Ashworth, P. J., J. L. Best, J. Peakall, and J. A. Lorson (1999), The influence of aggradation rate on braided alluvial architecture: Field study and physical scale modelling of the Ashburton River gravels, Canterbury Plains, New Zealand, in *Current Research in Fluvial Sedimentology: Proceedings of the 6th International Conference on Fluvial Sedimentology*, *Int. Assoc. Sedimentol. Spec. Publ. Ser.*, vol. 28, edited by N. D. Smith and J. J. Rogers, pp. 333–346, Int. Assoc. of Sedimentol., Boulder, Colo.

Ashworth, P. J., J. L. Best, and M. Jones (2004), Relationship between sediment supply and avulsion frequency in braided rivers, *Geology*, *32*(1), 21–24, doi:10.1130/G19919.1.

Barabasi, A. L., and H. E. Stanley (1995), *Fractal Concepts in Surface Growth*, 366 pp., Cambridge Univ. Press, New York.

Bates, C. C. (1953), Rational theory of delta formation, *Am. Assoc. Pet. Geol. Bull.*, *37*(9), 2119–2162.

Box, G. E. P., and G. M. Jenkins (1976), *Time Series Analysis: Forecasting and Control*, Holden-Day, San Francisco, Calif.

Bryant, M., P. Falk, and C. Paola (1995), Experimental study of avulsion frequency and rate of deposition, *Geology*, *23*, 365–368, doi:10.1130/0091-7613(1995)023<0365:ESOAFA>2.3.CO;2.

Cazanacli, D., C. Paola, and G. Parker (2002), Experimental steep, braided flow: Application to flooding risk on fans, *J. Hydraul. Eng.*, *128*(3), 322–330, doi:10.1061/(ASCE)0733-9429(2002)128:3(322).

Edmonds, D. A., and R. L. Slingerland (2007), Mechanics of river mouth bar formation: Implications for the morphodynamics of delta distributary networks, *J. Geophys. Res.*, *112*, F02034, doi:10.1029/2006JF000574.

Fagherazzi, S., A. Bortoluzzi, W. E. Dietrich, A. Adami, S. Lanzoni, M. Marani, and A. Rinaldo (1999), Tidal networks: 1. Automatic network extraction and preliminary scaling features from digital terrain maps, *Water Resour. Res.*, *35*(12), 3891–3904, doi:10.1029/1999WR900236.

Gardner, M. H., and J. M. Borer (2000), Submarine channel architecture along a slope-to-basin profile, Brushy Canyon Formation, west Texas, in *Fine-Grained Turbidity Systems*, *Am. Assoc. Pet. Geol. Mem. Ser.*, vol. 72, edited by A. H. Bouma and C. G. Stone, pp. 195–214, Am. Assoc. of Pet. Geol., Tulsa, Okla.

Gomez, B., R. L. Naff, and D. W. Hummell (1989), Temporal variations in bedload transport rates associated with the migration of bedforms, *Earth Surf. Processes Landforms*, *14*, 135–156, doi:10.1002/esp.3290140205.

Heller, P. L., and C. Paola (1996), Downstream changes in alluvial architecture: An exploration of controls on channel stacking patterns, *J. Sediment. Res.*, *66*, 297–306.

Hickson, T. A., B. A. Sheets, C. Paola, and M. Kelberer (2005), Experimental test of tectonic controls on three-dimensional alluvial facies architecture, *J. Sediment. Res.*, *75*, 710–722, doi:10.2110/jsr.2005.057.

Hoyal, D. C. J. D., and B. A. Sheets (2009), Morphodynamic evolution of experimental cohesive deltas, *J. Geophys. Res.*, *114*, F02009, doi:10.1029/2007JF000882.

Jerolmack, D. J., and D. Mohrig (2005), A unified model for subaqueous bed form dynamics, *Water Resour. Res.*, *41*, W12421, doi:10.1029/2005WR004329.

Jerolmack, D. J., and D. Mohrig (2007), Conditions for branching in depositional rivers, *Geology*, *35*(5), 463–466, doi:10.1130/G23308A.1.

Jerolmack, D. J., and C. Paola (2007), Complexity in a cellular model of river avulsion, *Geomorphology*, *91*, 259–270, doi:10.1016/j.geomorph.2007.04.022.

Jerolmack, D. J., and J. B. Swenson (2007), Scaling relationships and evolution of distributary networks on wave-influenced deltas, *Geophys. Res. Lett.*, *34*, L23402, doi:10.1029/2007GL031823.

Kim, W., and C. Paola (2007), Long-period cyclic sedimentation with constant tectonic forcing in an experimental relay ramp, *Geology*, *35*(4), 331–334, doi:10.1130/G23194A.1.

Kim, W., C. Paola, J. B. Swenson, and V. R. Voller (2006), Shoreline response to autogenic processes of sediment storage and release in the fluvial system, *J. Geophys. Res.*, *111*, F04013, doi:10.1029/2006JF000470.

Leeder, M. R. (1978), A quantitative stratigraphic model for alluvium, with special reference to channel deposit density and interconnectedness, in *Fluvial Sedimentology*, edited by A. D. Miall, pp. 587–596, Canadian Society of Petroleum Geologists, Calgary, Alberta, Canada.

Leeder, M. R., G. H. Mack, J. Peakall, and S. Salyards (1996), First quantitative test of alluvial stratigraphic models: Southern Rio Grande rift, New Mexico, *Geology*, *24*(1), 87–90, doi:10.1130/0091-7613(1996)024<0087:FQTOAS>2.3.CO;2.

Mohrig, D., P. L. Heller, C. Paola, and W. J. Lyons (2000), Interpreting avulsion process from ancient alluvial sequences: Guadalope-Matarranya system (northern Spain) and Wasatch Formation (western Colorado), *Geol. Soc. Am. Bull.*, *112*(12), 1787–1803, doi:10.1130/0016-7606(2000)112<1787:IAPFAA>2.0.CO;2.

Morisawa, M. (1985), *Rivers, Form and Process*, 232 pp., Longman, London.

Nikora, V. I., A. N. Sukhodolov, and P. M. Rowinski (1997), Statistical sand wave dynamics in one-directional water flows, *J. Fluid Mech.*, *351*, 17–39, doi:10.1017/S0022112097006708.

Paola, C. (2001), Modelling stream braiding over a range of scales, in *Gravel Bed Rivers V*, edited by M. P. Mosley, pp. 11–46, N. Z. Hydrol. Soc., Wellington.

Paola, C., and E. Foufoula-Georgiou (2001), Statistical geometry and dynamics of braided rivers, in *Gravel Bed Rivers V*, edited by M. P. Mosley, pp. 47–71, N. Z. Hydrol. Soc., Wellington.

Paola, C., P. L. Heller, and C. L. Angevine (1992), The large-scale dynamics of grain-size variation in alluvial basins, part 1: Theory, *Basin Res.*, *4*, 73–90.

Paola, C., G. Parker, D. C. Mohrig, and K. X. Whipple (1999), The influence of transport fluctuations on spatially averaged topography on a sandy, braided fluvial fan, in *Numerical Experiments in Stratigraphy: Recent Advances in Stratigraphic and Sedimentologic Computer Simulations*, *Soc. Econ. Paleontol. Mineral. Spec. Publ. Ser.*, vol. 62, edited by J. Harbaugh et al., pp. 211–218, Soc. of Econ. Paleontol. and Mineral., Tulsa, Okla.

Peakall, J., M. R. Leeder, J. L. Best, and P. J. Ashworth (2000), River response to lateral ground tilting: A synthesis and some implications for the modeling of alluvial architecture in extensional basins, *Basin Res.*, *12*, 413–424, doi:10.1046/j.1365-2117.2000.00128.x.

Sheets, B., T. Hickson, and C. Paola (2002), Assembling the stratigraphic record: Depositional patterns and time-scales in an experimental alluvial basin, *Basin Res.*, *14*, 287–301, doi:10.1046/j.1365-2117.2002.00185.x.

Sheets, B. A., C. Paola, and J. M. Kelberer (2007), Creation and preservation of channel-form sand bodies in an experimental alluvial system, in *Sedimentary Processes, Environments and Basins: A Tribute to Peter Friend*, *Int. Assoc. Sedimentol. Spec. Publ. Ser.*, vol. 38, edited by G. J. Nichols, E. Williams, and C. Paola, pp. 555–657, Blackwell, Malden, Mass.

Slingerland, R., and N. D. Smith (1998), Necessary conditions for a meandering-river avulsion, *Geology*, *26*(5), 435–438, doi:10.1130/0091-7613(1998)026<0435:NCFAMR>2.3.CO;2.

Slingerland, R., and N. D. Smith (2004), River avulsions and their deposits, *Annu. Rev. Earth Planet. Sci.*, *32*, 257–285, doi:10.1146/annurev.earth.32.101802.120201.

Sun, T., C. Paola, and G. Parker (2002), Fluvial fan deltas: Linking channel processes with large-scale morphodynamics, *Water Resour. Res.*, *38*(8), 1151, doi:10.1029/2001WR000284.

Swenson, J. B. (2005), Relative importance of fluvial input and wave energy in controlling the timescale for distributary-channel avulsions, *Geophys. Res. Lett.*, *32*, L23404, doi:10.1029/2005GL024758.

Swenson, J. B., V. R. Voller, C. Paola, G. Parker, and J. G. Marr (2000), Fluvio-deltaic sedimentation: A generalized Stefan problem, *Eur. J. Appl. Math.*, *11*, 433–452, doi:10.1017/S0956792500004198.

Tornqvist, T. E. (1994), Middle and late Holocene avulsion history of the River Rhine (Rhine-Meuse delta, Netherlands), *Geology*, *22*, 711–714, doi:10.1130/0091-7613(1994)022<0711:MALHAH>2.3.CO;2.

Tornqvist, T. E., and J. S. Bridge (2002), Spatial variation in overbank aggradation rate and its influence on avulsion frequency, *Sedimentology*, *49*, 891–905, doi:10.1046/j.1365-3091.2002.00478.x.

Wickert, A. (2007), Measuring channel mobility through the analysis of area-based change in analog experiments, with insights into alluvial environments, S.B. thesis, 128 pp., Mass. Inst. of Technol., Cambridge, Mass.

Wright, J. M., and L. D. Coleman (1973), Variations in morphology of major river deltas as functions of wave and river discharge regimes, *Am. Assoc. Pet. Geol. Bull.*, *57*(2), 370–398.

Wright, L. D. (1977), Sediment transport and deposition at river mouths: A synthesis, *Geol. Soc. Am. Bull.*, *88*(6), 857–868, doi:10.1130/0016-7606(1977)88<857:STADAR>2.0.CO;2.

D. Hoyal, J. Martin, and B. Sheets, ExxonMobil Upstream Research Company, P.O. Box 2189, Houston, TX 77252, USA. (john.m.martin@exxonmobil.com)

C. Paola, St. Anthony Falls Laboratory, University of Minnesota, 2 Third Avenue, SE, Minneapolis, MN 55414, USA.